Harmonic experiments to model fracture induced anisotropy

KAUST-IAMCS WORKSHOP on Modeling and Simulation of Wave Propagation and Applications,

Thuwal, Kindom of Saudi Arabia, May 8-9, 2012

Juan E. Santos,[†]

[†] Department of Mathematics, Purdue University, West Lafayette, Indiana, USA, Instituto del Gas y del Petróleo (IGPUBA), Universidad de Buenos Aires, Argentina, and Universidad Nacional de La Plata, Argentina.

work in collaboration with J. M. Carcione and S. Picotti, (OGS), Trieste, Italy.

Fractured media. I

- Fractures are common in the earth's crust due to different factors, for instance, tectonic stresses and natural or artificial hydraulic fracturing caused by a pressurized fluid.
- Seismic wave propagation through fractures and cracks is an important subject in exploration and production geophysics, earthquake seismology and mining.
- Fractures constitute the sources of earthquakes, and hydrocarbon and geothermal reservoirs are mainly composed of fractured rocks.

Fractured media. II

- Modeling fractures requires a suitable interface model. Schoenberg (JASA (1980), GP (1983)) proposed the so-called linear-slip boundary condition model (LSBC), based on the discontinuity of the displacement across the fractures. (Schoenberg's model).
- A generalization of the (LSBC) (Carcione, JGR (1996)) states that across a fracture stress components are proportional to the displacement and velocity discontinuities through the specific stiffnesses and specific (viscosities, respectively.

Fractured media. III

- Displacement discontinuities conserve energy, while velocity discontinuities generate energy loss at the fractures. The specific viscosity accounts for the presence of a liquid under saturated conditions, introducing a viscous coupling between both sides of a fracture.
- Schoemberg's theory predicts that a dense set of parallel plane fractures behaves as a Transversely Isotropic Viscoelastic (TIV) medium if the dominant wavelength of the traveling waves is much larger than the distance between the fractures.

Fractured media. IV

- Schoenberg's model has never been simulated with a numerical method.
- To test the theory, in the context of Numerical rock physics we developped a novel numerical solver that can be used in more general situations.
- Numerical rock physics offer an alternative to laboratory measurements.
- Numerical experiments are inexpensive, repeatable, essentially free from experimental errors and can easily be run using alternative models of the materials being analized.

Fractured media. V

- To determine the complex stiffness coefficients of the equivalent TIV medium, we solve a set of boundary value problems (BVP's) for the wave equation of motion in the frequency-domain using the finite-element method (FEM).
- The BVP's represent harmonic tests at a finite number of frequencies on a sample having a dense set of fractures, modeled using the LSBC.

The equivalent TIV medium. I

Consider a viscoelastic isotropic background medium having a set of parallel (horizontal) fractures and its description in the space-frequency domain.

$\mathbf{u}$, $e_{ij}(\mathbf{u}), \sigma_{ij}(\mathbf{u})$: frequency domain displacement vector, strain components and stress components of the background medium.

The stress-strain relations and equations of motion:

$$\sigma_{jk}(\mathbf{u}) = \lambda\delta_{jk}\nabla\cdot\mathbf{u} + 2\mu e_{jk}(\mathbf{u})$$

$$\rho\omega^2\mathbf{u}(x,z,\omega) + \nabla\cdot\boldsymbol{\sigma}[\mathbf{u}(x,z,\omega)] = 0$$

δ_{jk}: Kroenecker delta λ, μ: complex Lamé constants ρ: mass density.

The equivalent TIV medium. II

x_1 **and** x_3**: horizontal and vertical coordinates, respectively.**

When a dense set of parallel fractures is present, the medium behaves as a TIV medium with x_3**-axis of symmetry at long wavelengths.**

τ_{ij}, ϵ_{ij}**: stress and strain tensors of the equivalent TIV medium**

Stress-strain relations:

$$\tau_{11}(\mathbf{u}) = p_{11}\,\epsilon_{11}(\mathbf{u}) + p_{12}\,\epsilon_{22}(\mathbf{u}) + p_{13}\,\epsilon_{33}(\mathbf{u}), \tag{1}$$

$$\tau_{22}(\mathbf{u}) = p_{12}\,\epsilon_{11}(\mathbf{u}) + p_{11}\,\epsilon_{22}(\mathbf{u}) + p_{13}\,\epsilon_{33}(\mathbf{u}), \tag{2}$$

$$\tau_{33}(\mathbf{u}) = p_{13}\,\epsilon_{11}(\mathbf{u}) + p_{13}\,\epsilon_{22}(\mathbf{u}) + p_{33}\,\epsilon_{33}(\mathbf{u}), \tag{3}$$

$$\tau_{23}(\mathbf{u}) = 2\,p_{55}\,\epsilon_{23}(\mathbf{u}), \tag{4}$$

$$\tau_{13}(\mathbf{u}) = 2\,p_{55}\,\epsilon_{13}(\mathbf{u}), \quad \tau_{12}(\mathbf{u}) = 2\,p_{66}\,\epsilon_{12}(\mathbf{u}). \tag{5}$$

Schoenberg's theory predicts that if the background medium is homogeneous, the stiffnesses $\mathbf{p_{IJ}}$'s are given by

$$p_{11} = p_{22} = E - \lambda^2 Z_N c_N, \quad p_{12} = \lambda - \lambda^2 Z_N c_N \quad p_{13} = \lambda c_N, \tag{6}$$
$$p_{33} = E c_N, \quad p_{55} = \mu c_T, \quad p_{66} = \mu.$$

where

$$c_N = (1 + E Z_N)^{-1} \ \text{ and } \ c_T = (1 + \mu Z_T)^{-1},$$

$\mathbf{Z_N}$ and $\mathbf{Z_T}$: normal and tangential complex compliances of the fractures
$E = \lambda + 2\mu$.

The equivalent TIV medium. IV

The theory assumes that that distance between fractures is much smaller than the wavelength of the signal and that the boundary condition is the same for all the fractures.

Moreover, the theory assumes that the fracture distance is constant.

The numerical solver may consider an inhomogeneous background medium, unequal fracture distances and dissimilar boundary conditions at the fractures surfaces.

The p_{IJ}'s are the complex and frequency-dependent stiffnesses to be determined numerically with the harmonic experiments.

Determination of the stiffness components $\mathrm{p_{IJ}}$

$\Omega = (0, D)^2$: **a square sample of boundary** $\Gamma = \Gamma^L \cup \Gamma^R \cup \Gamma^B \cup \Gamma^T$, **where**

$$\Gamma^L = \{(x,z) \in \Gamma : x = 0\}, \quad \Gamma^R = \{(x,z) \in \Gamma : x = D\},$$
$$\Gamma^B = \{(x,z) \in \Gamma : z = 0\}, \quad \Gamma^T = \{(x,z) \in \Gamma : z = D\}.$$

$\Gamma^{(f,l)}, l = 1, \cdots, J^{(f)}$: **a set of** $J^{(f)}$ **horizontal fractures each one of length** D **in our domain** Ω.

This set of fractures divides Ω **in a set of nonoverlapping rectangles** $R^{(l)}, l = 1, \cdots, J^f + 1$, **so that**

$$\Omega = \cup_{l=1}^{J^{(f)}+1} R^{(l)}.$$

Boundary conditions at the fractures. I

Consider a fracture $\Gamma^{(f,l)}$ and the two rectangles $R^{(l)}$ and $R^{(l+1)}$ having as a common side $\Gamma^{(f,l)}$.

$\mathbf{n}_{l,l+1}, \mathbf{m}_{l,l+1}$: the unit outer normal and a unit tangent (oriented counterclockwise) on $\Gamma^{(f,l)}$ from $R^{(l)}$ to $R^{(l+1)}$, such that $\{\mathbf{n}_{l,l+1}, \mathbf{m}_{l,l+1}\}$ is an orthonormal system on $\Gamma^{(f,l)}$.

Set $\mathbf{u}^{(l)} = \mathbf{u}|_{R^{(l)}}$: restriction of $\mathbf{u}$ to $R^{(l)}$, and let

$$[\mathbf{u}] = \left(\mathbf{u}^{(l)} - \mathbf{u}^{(l+1)}\right)|_{\Gamma^{(f,l)}}$$

denote the jump of $\mathbf{u}$ at $\Gamma^{(f,l)}$

Boundary conditions at the fractures. II

The boundary conditions (B.C.) at the fractures $\Gamma^{(f,l)}$ are the stress continuity and the condition that stress components be proportional to the displacement and velocity discontinuities through specific stiffnesses and viscosities, respectively. Thus,

$$\boldsymbol{\sigma}(\mathbf{u}^{(l)})\mathbf{n}_{l,l+1} = \boldsymbol{\sigma}(\mathbf{u}^{(l+1)})\mathbf{n}_{l,l+1} \quad \Gamma^{(f,l)}, \tag{7}$$

$$\left(\boldsymbol{\sigma}(\mathbf{u}^{(l)})\mathbf{n}_{l,l+1} \cdot \mathbf{n}_{l,l+1}, \boldsymbol{\sigma}(\mathbf{u}^{(l)})\mathbf{n}_{l,l+1} \cdot \mathbf{m}_{l,l+1}\right)^T$$

$$= \mathbf{S}^{(l)}(\omega)\left([\mathbf{u}] \cdot \mathbf{n}_{l,l+1}, [u] \cdot \mathbf{m}_{l,l+1}\right)^T \quad \Gamma^{(f,l)},\ l = 1, \cdots, J^{(f)}. \tag{8}$$

where T indicates the transpose.

Boundary conditions at the fractures. III

If L denotes the average distance between the fractures, the matrix $\mathbf{S}^{(l)}(\omega)$ has the form

$$\mathbf{S}^{(l)}(\omega) = \begin{pmatrix} (LZ_N^l)^{-1} & 0 \\ 0 & (LZ_T^{(l)})^{-1} \end{pmatrix} \tag{9}$$

The compliances Z (Z_N or Z_T) are complex and frequency-dependent and can be expressed as

$$Z^{-1} = L(\kappa + \mathrm{i}\omega\eta),$$

where κ is a specific stiffness and η is a specific viscosity, having dimensions of stiffness and viscosity per unit length, respectively.

Determination of the stiffness components $\mathrm{p_{IJ}}$. I

For p_{33} we solve solve the wave equation in Ω using the fracture B. C.'s with the additional B. C.'s

$$\boldsymbol{\sigma}(\mathbf{u})\mathbf{n}\cdot\mathbf{n} = -\Delta P, \quad \Gamma^T, \tag{10}$$

$$\boldsymbol{\sigma}(\mathbf{u})\mathbf{n}\cdot\mathbf{m} = 0, \quad \Gamma, \tag{11}$$

$$\mathbf{u}\cdot\nu = 0, \quad \Gamma^L \cup \Gamma^R \cup \Gamma^B. \tag{12}$$

In this experiment $\epsilon_{11}(\mathbf{u}) = \epsilon_{22}(\mathbf{u}) = 0$.

Determination of the stiffness components p_{IJ}. II

Denoting by V the original volume of the sample, its (complex) oscillatory volume change, $\Delta V(\omega)$, we note that in the quasistatic case

$$\frac{\Delta V(\omega)}{V} = -\frac{\Delta P}{p_{33}(\omega)},$$

The computed average vertical displacement $u_3^{s,T}(\omega)$ suffered by the boundary Γ^T allows us to use the estimate

$$\Delta V(\omega) \approx D u_3^{s,T}(\omega),$$

from where we can determine $p_{33}(\omega)$.

Determination of the stiffness components p_{IJ}. III

For p_{11} we solve the wave equation with the fracture B. C.'s and the additional B. C.'s

$$\boldsymbol{\sigma}(\mathbf{u}) \cdot \mathbf{n} \cdot \mathbf{n} = -\Delta P, \quad \Gamma^R,$$

$$\boldsymbol{\sigma}(\mathbf{u}) \cdot \mathbf{n} \cdot \mathbf{m} = 0, \quad \Gamma,$$

$$\mathbf{u} \cdot \mathbf{n} = 0, \quad \Gamma^L \cup \Gamma^B \cup \Gamma^T.$$

In this experiment, ϵ_{33} = ϵ_{22} = 0 and this experiment determines p_{11} computing the volume change in the same way indicated for p_{33}.

For p_{55} we solve the wave equation with the fracture B. C.'s and the additional B. C.'s

$$\boldsymbol{\sigma} \cdot \mathbf{m} = \mathbf{g}, \quad \Gamma^T \cup \Gamma^L \cup \Gamma^R,$$
$$\mathbf{u} = 0, \quad \Gamma^B,$$

where

$$\mathbf{g} = \begin{cases} (0, \Delta G), & \Gamma^L, \\ (0, -\Delta G), & \Gamma^R, \\ (\Delta G, 0), & \Gamma^T. \end{cases}$$

Determination of the stiffness components $\mathrm{p_{IJ}}$. V

Let $\theta(\omega)$: **angle between the original positions of the lateral boundaries and the location after applying the shear stresses.**

To estimate $\theta(\omega)$, **we compute the average horizontal displacement** $\mathbf{u}_1^T(\omega)$ **at the boundary** Γ^T **and use that**

$$\tan[\theta(\omega)] \approx \mathbf{u}_1^T(\omega)/D.$$

Thus, the change in shape of the rock sample allow us to determine $p_{55}(\omega)$ **from the relation (Kolsky, 1963)**

$$\tan[\theta(\omega)] = \frac{\Delta G}{p_{55}(\omega)}.$$

Determination of the stiffness components p_{IJ}. V

For p_{13} we solve the wave equation with the fracture B. C.'s and the additional B. C.'s

$$\boldsymbol{\sigma}(\mathbf{u}) \cdot \mathbf{n} \cdot \mathbf{n} = -\Delta P, \quad \Gamma^R \cup \Gamma^T,$$

$$\boldsymbol{\sigma}(\mathbf{u}) \cdot \mathbf{n} \cdot \mathbf{m} = 0, \quad \Gamma,$$

$$\mathbf{u} \cdot \mathbf{n} = 0, \quad \Gamma^L \cup \Gamma^B.$$

In this experiment ϵ_{22} = 0, and from the stress-strain relations at the macroscale we get

Determination of the stiffness components p_{IJ}. V

$$\tau_{11} = p_{11}\epsilon_{11} + p_{13}\epsilon_{33},$$

$$\tau_{33} = p_{13}\epsilon_{11} + p_{33}\epsilon_{33},$$

$\epsilon_{11}, \epsilon_{33}$: macroscopic strain components at the right lateral side and top side of the sample, respectively.

Then using that $\tau_{11} = \tau_{33} = -\Delta P$ we obtain

$$p_{13}(\omega) = \frac{p_{11}\epsilon_{11} - p_{33}\epsilon_{33}}{\epsilon_{11} - \epsilon_{33}}.$$

A variational formulation

Test space fo $\mathbf{p_{33}}(\omega)$:

$$\mathcal{W}_{33}(\Omega) = \{v \in [L^2(\Omega)]^2 : v|_{R^{(l)}} \in [H^1(R^{(l)})]^2,\ v \cdot \nu = 0 \text{ on } \Gamma^L \cup \Gamma^R \cup \Gamma^B\},$$

To determine $\mathbf{p_{33}}(\omega)$: find $\mathbf{u^{(33)}} \in \mathcal{W}_{33}(\Omega)$ such that:

$$-\omega^2(u,v) + \sum_{l=1}^{J^{(f)}+1} \sum_{s,t=1,3} (\sigma_{st}(u), \epsilon_{st}(v))_{R^{(l)}} \tag{13}$$

$$+ \sum_{l=1}^{J^{(f)}} \left[\left\langle [LZ_N^{(l)}]^{-1}[u]_3, [v]_3 \right\rangle_{\Gamma^{(f,l)}} + \left\langle [LZ_T^{(l)}]^{-1}[u]_1, [v]_1 \right\rangle_{\Gamma^{(f,l)}} \right]$$

$$= -\langle \Delta P, v \cdot \nu \rangle_{\Gamma^T}, \qquad \forall v \in \mathcal{W}_{33}(\Omega). \tag{14}$$

Similar formulations hold for the other $\mathbf{p_{IJ}}$'s

Finite element implementation

The FE variational formulation uses **bilinear elements** to compute approximate solution of the BVP, and is explained in Santos et al. (CMAME, 2012, submittted), where apriori error estimates which are optimal for the regularity of the solution are given.

Results on the existence and uniqueness of the continuous and discrete BVP's are also given in that reference.

The **error** is of the order of h in the L^2**-norm** and of the order of $h^{1/2}$ both in the **interior energy norm** and in the L^2**-norm** on the set of fractures, where h **is the diameter** of the elements.

Numerical experiments.

We consider the data provided by the laboratory experiments of Chichinina et al. (TPM, 2009). The background medium is isotropic with λ = 10 GPa, μ = 3.9 GPa and ρ = 2300 kg/m^3.

The simulations to determine the $\mathbf{p_{IJ}}$'s have fracture distance L =1 cm, grid spacing h = 0.5 cm and a frequency f_0 = 25 Hz.

$\mathbf{p_{11}}$, $\mathbf{p_{13}}$ and $\mathbf{p_{33}}$: 29 equally spaced fractures, 60×60 mesh.

$\mathbf{p_{55}}$: 14 fractures, 30×30 mesh.

Experimental values of $\mathbf{Z_N}$ and $\mathbf{Z_T}$ for wet fractures scaled to seismic frequencies:

$\mathbf{Z_N^{-1}}$ = [34 + $\mathrm{i}(f/f_0)$ 24.7] GPa $\mathbf{Z_T^{-1}}$ = [15.5 + $\mathrm{i}(f/f_0)$ 11.3] GPa

Determination of reliable fracture parameters needs measurements at the seismic range (experimental data was obtained at 100 kHz).

Validation of the FE method. Phase velocities as function of frequency for wet fr

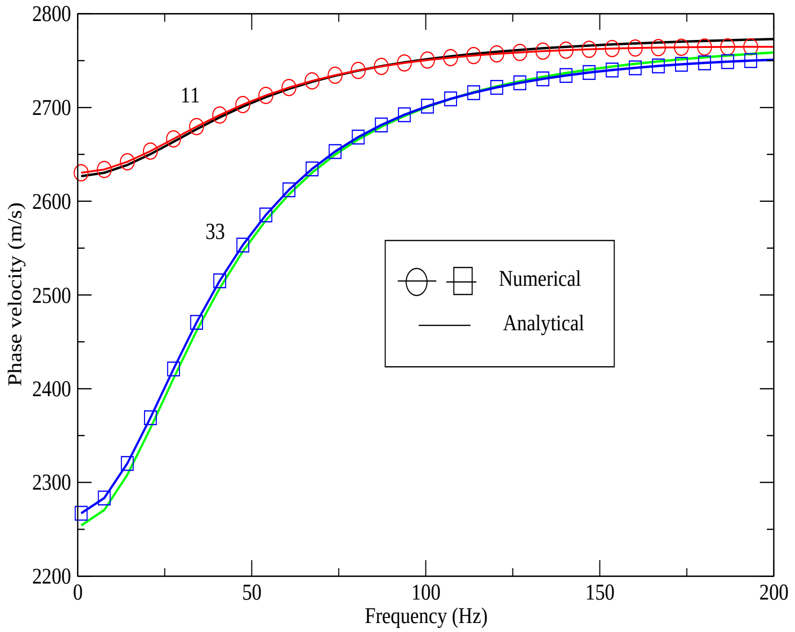

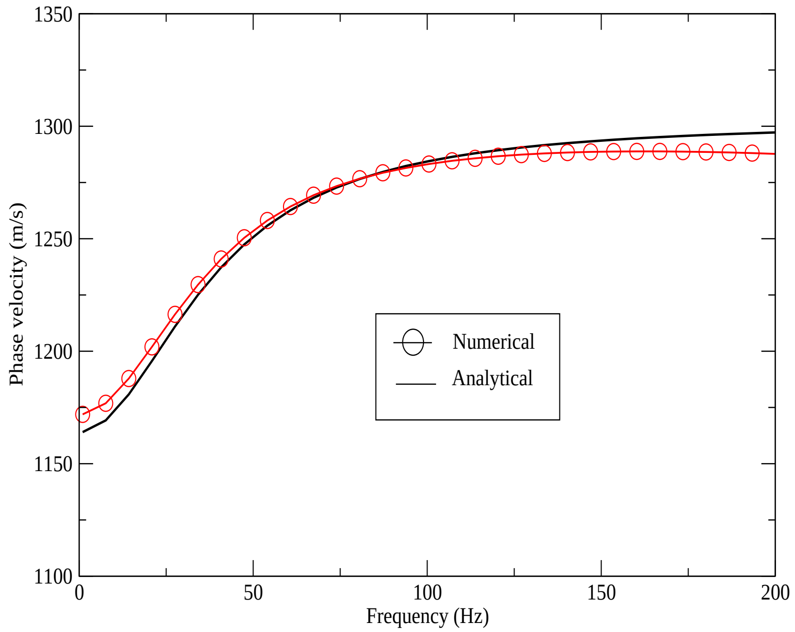

“11” and “33” refer to the qP wave along and perpendicular to the fracture plane. “55” refers to the qS wave perperdicular to the fracture plane. A very good fit is observed. qP waves along the fracture plane (“11”) travel faster than qP waves travelling perpendicular to the fractures (“33”).

Validation of the FE method. Dissipation factor as function of frequency for wet

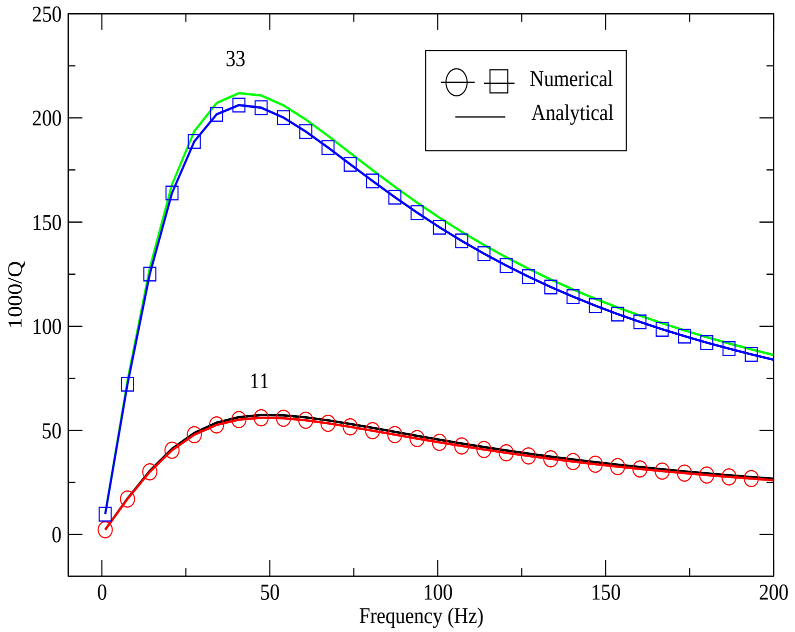

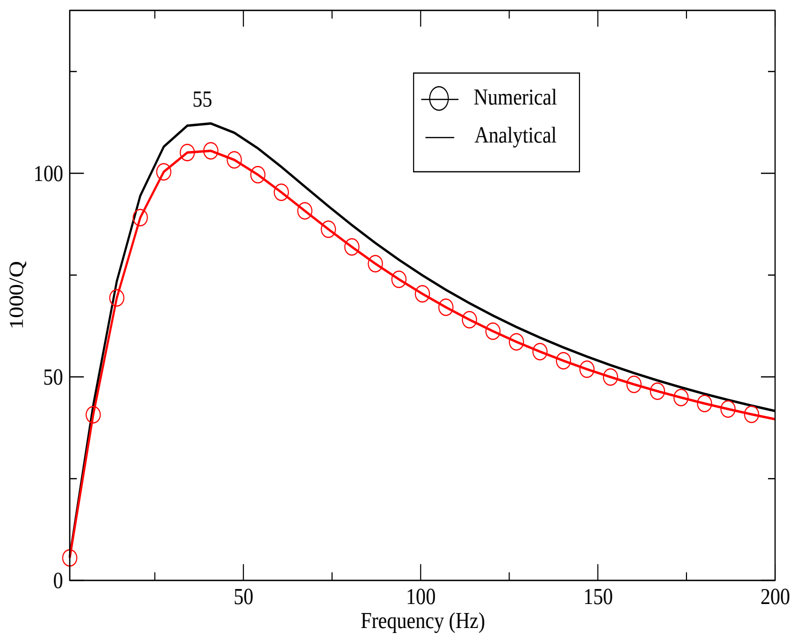

"11" and "33" refer to the qP wave along and perpendicular to the fracture plane. "55" and "66" refer to the qS and SH waves perperdicular and along the fracture plane. The SH wave is lossless. A very good fit is observed. qP waves along the fracture plane ("11") suffer lower attenuation than qP waves travelling perpendicular to the fractures ("33").

Fractures at varying pore fluid pressure .

Daley et a. (GPY, 2006) suggest to take high values of fracture compliance at low normal effective stress $\sigma = pc - pp$, where pc is the confining pressure and pp the prore presure.

For a contant pc = 30 MPa, we consider two pore pressures 5 MPa and 25 MPa, normal and overpressure values, respectively. Using their model, we obtain, at 25 Hz,

$$pp = 5 \text{ MPa}, \quad Z_N^{-1} = (23.1 + 5.9\mathrm{i}) \text{ GPa}, \quad Z_T^{-1} = (75 + 9.4\mathrm{i}) \text{ GPa},$$
$$pp = 28 \text{ MPa}, \quad Z_N^{-1} = (14.4 + 3.6\mathrm{i}) \text{ GPa}, \quad Z_T^{-1} = (21 + 2.6\mathrm{i}) \text{ GPa},$$

We consider a set of equispaced fractures with L = 1 cm and 80 % binary fractal variations of Z_N and Z_T around these mean values.

Real part of fractal $\mathrm{Z}_{\mathrm{N}}^{-1}$ at pore pressure 28 MPa.

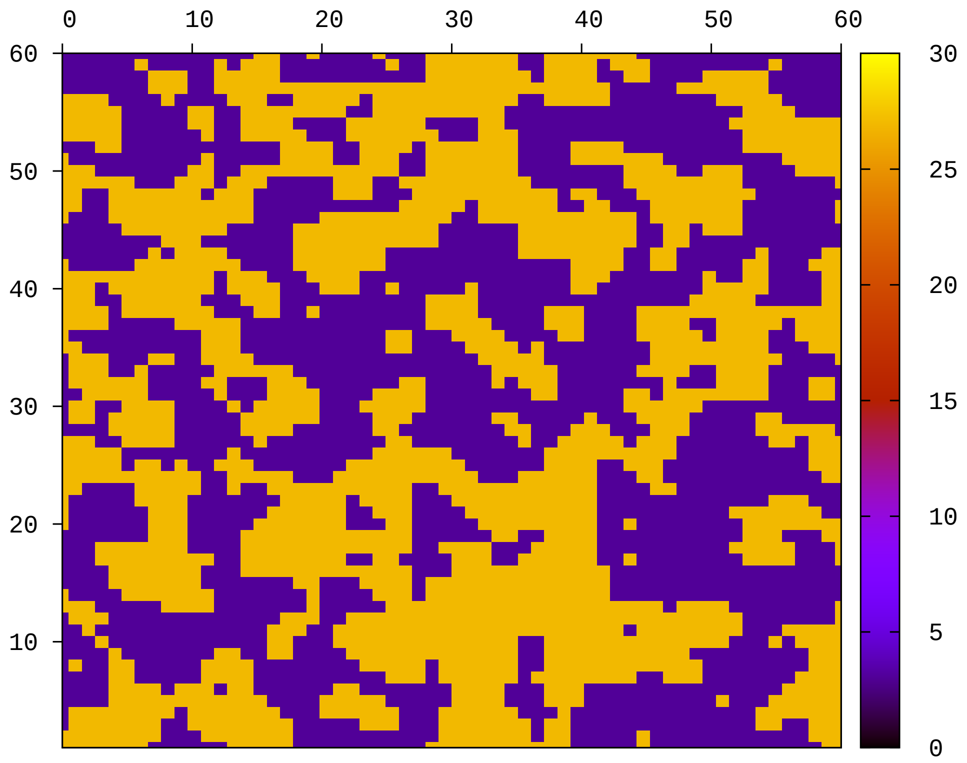

80 % binary fractal variations of Z_N around the mean value 23.1 GPa

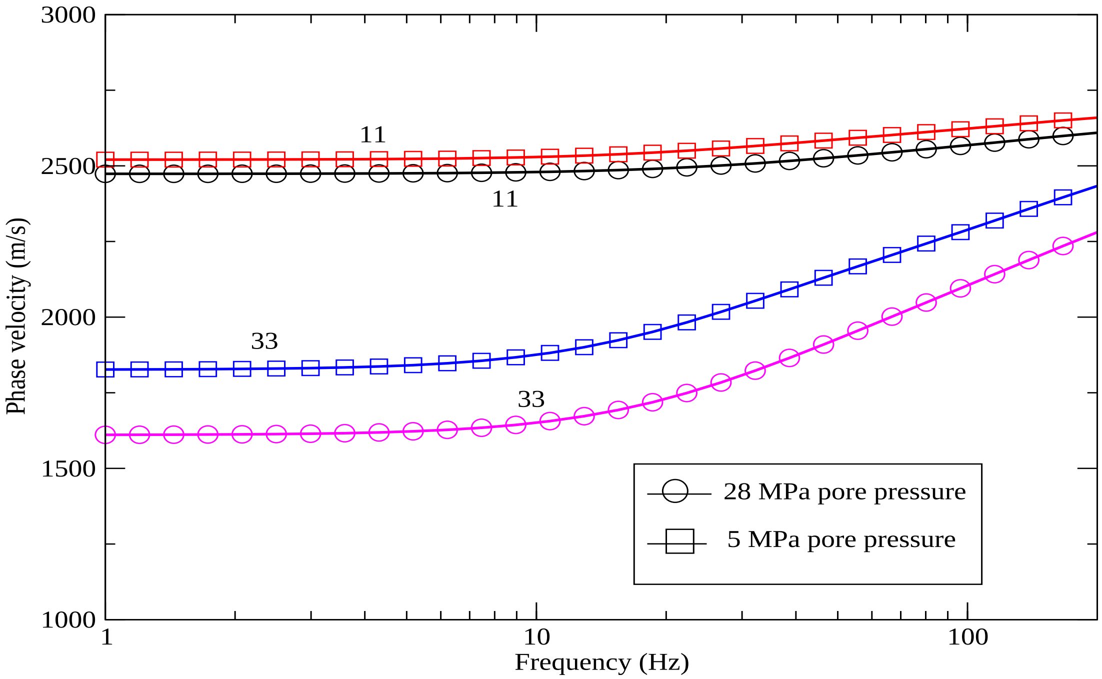

$\sigma = pc - pp$ is the effective normal stress, pc = confining pressure, pp= pore pressure. “11” and “33” refer to the qP wave along and perpendicular to the fracture plane. Higher pore pressure (circles) implies lower phase velocity. The “33” qP wave is the one more affected by overpressure.

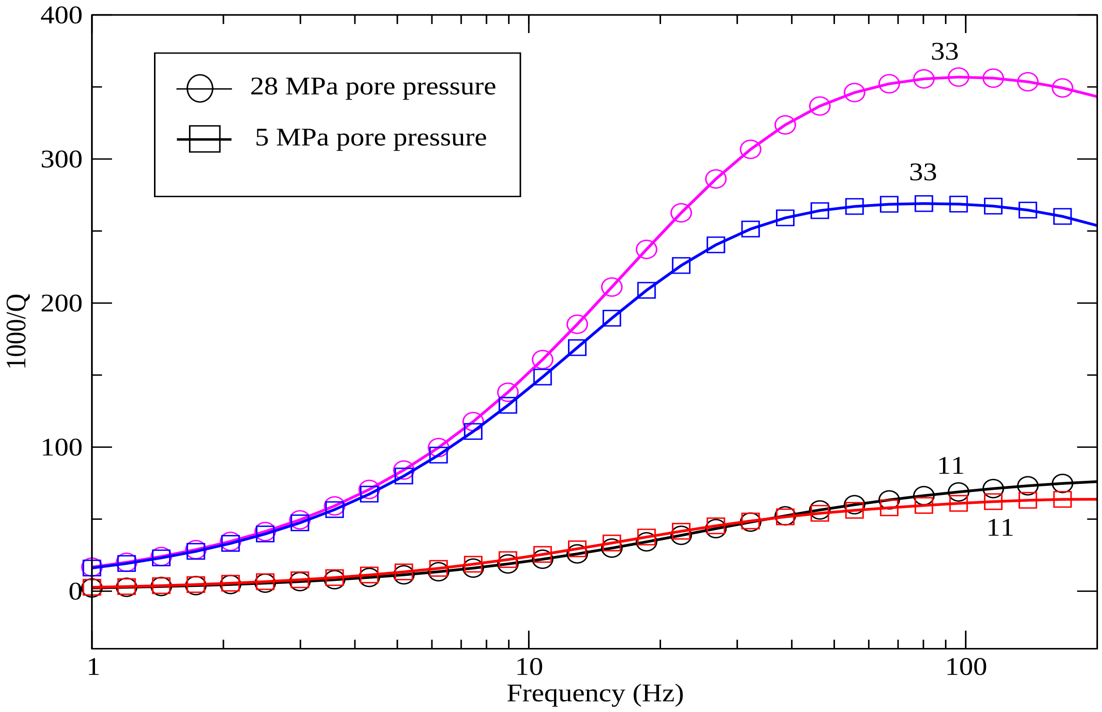

$\sigma = pc - pp$ is the effective normal stress, pc = confining pressure, pp= pore pressure. “11” and “33” refer to the qP wave along and perpendicular to the fracture plane. Attenuation is stronger in the overpressured case (circles) for “33” waves.

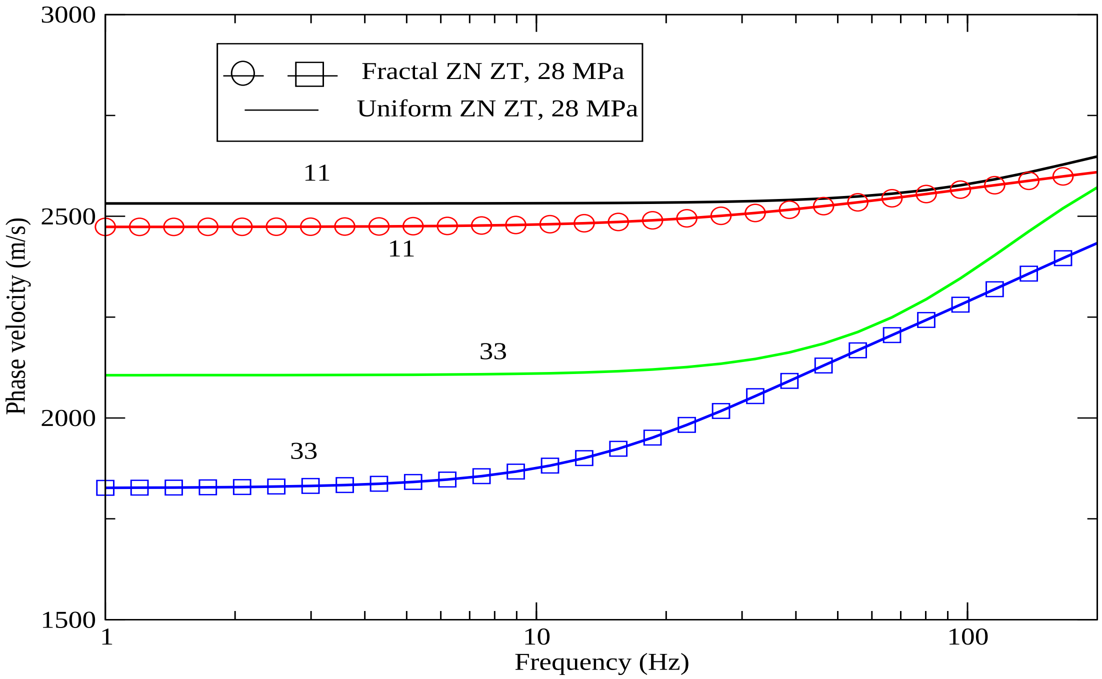

“11” and “33” refer to the qP wave along and perpendicular to the fracture plane. Phase velocities in the fractal case are lower than those obtained with the mean values. The “33” qP wave is the one more affected by the heterogeneities.

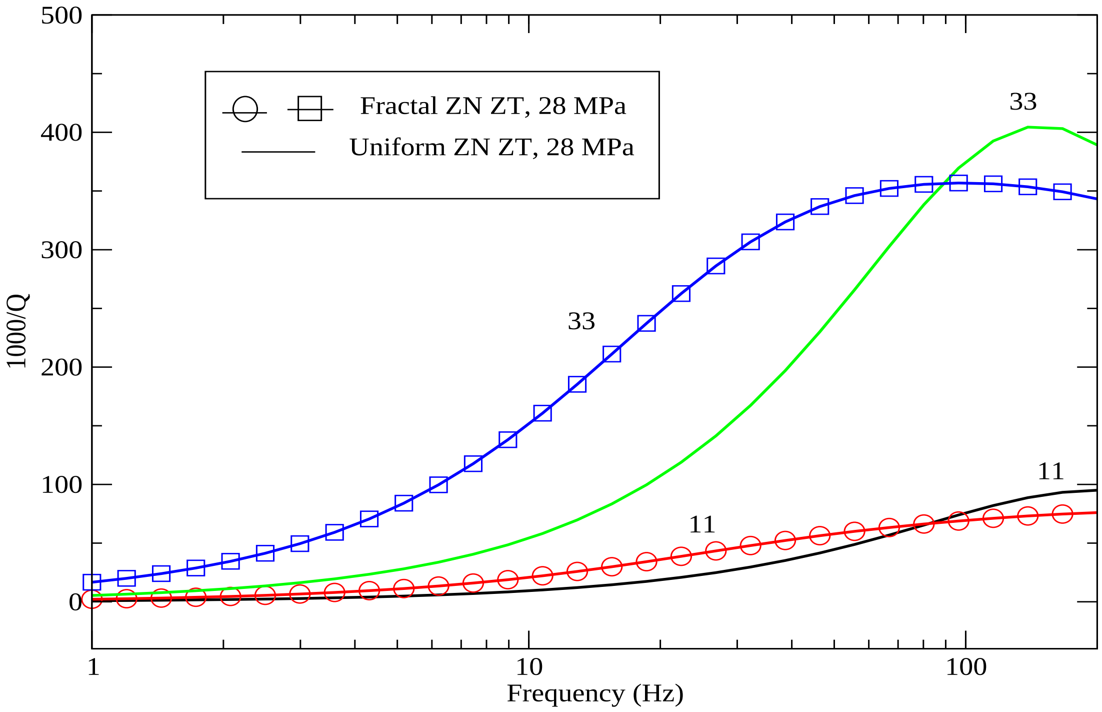

"11" and "33" refer to the qP wave along and perpendicular to the fracture plane. Dissipation factor of the "33" qP wave is more affected by the heterogeneities, showing lower values in the fractal case.

Fractal λ and μ background.

Next we consider 50 % binary fractal variations of the background Lamé constants λ and μ with respect to the mean values 10 GPa and 3.9 GPa, respectively.

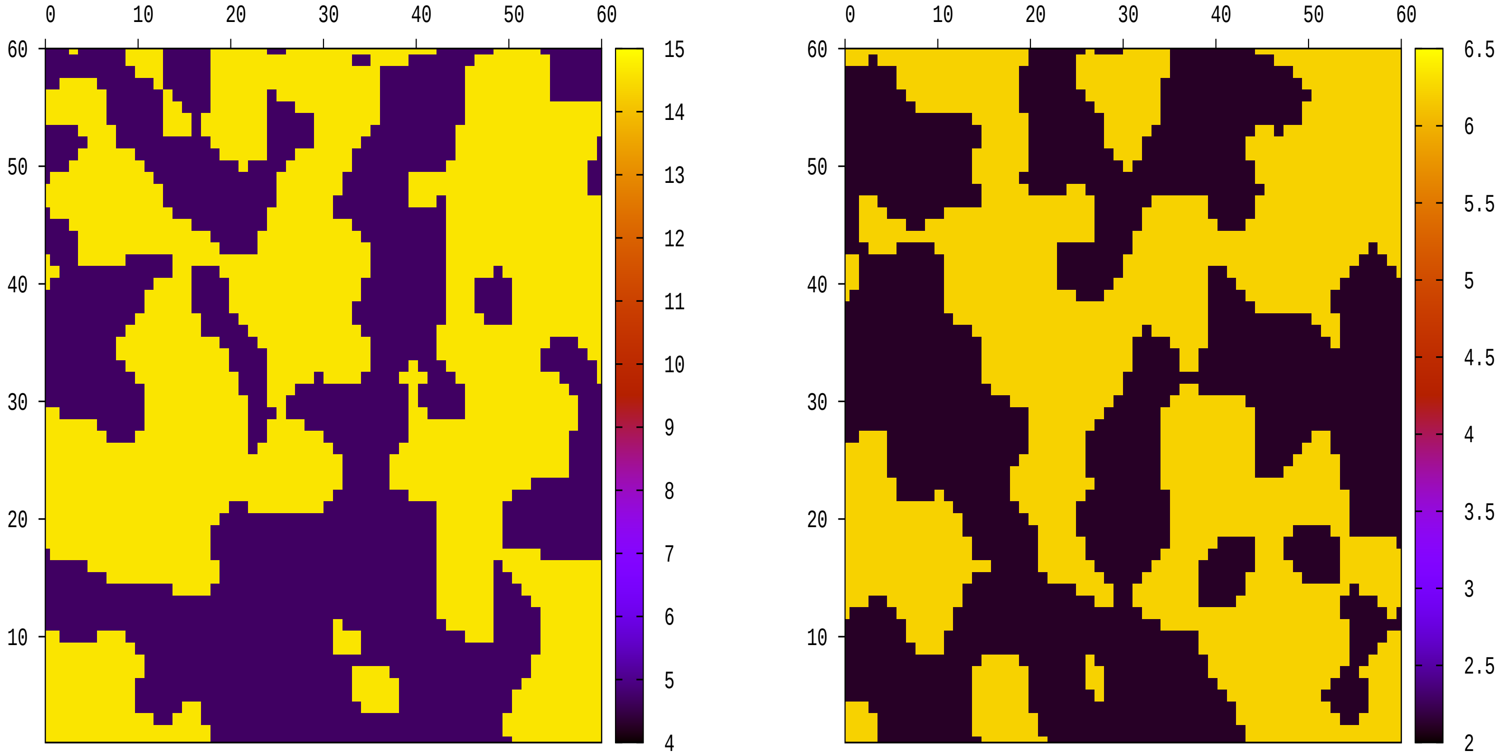

Phase velocities and dissipation as function of frequency. Uniform and fractal brackground, dry fractures: Z_N^{-1} = 9.6 +

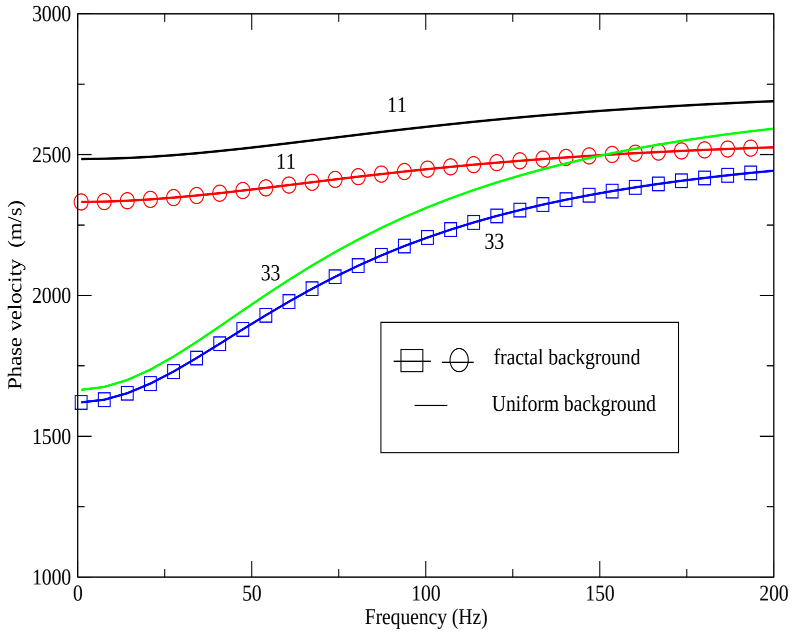

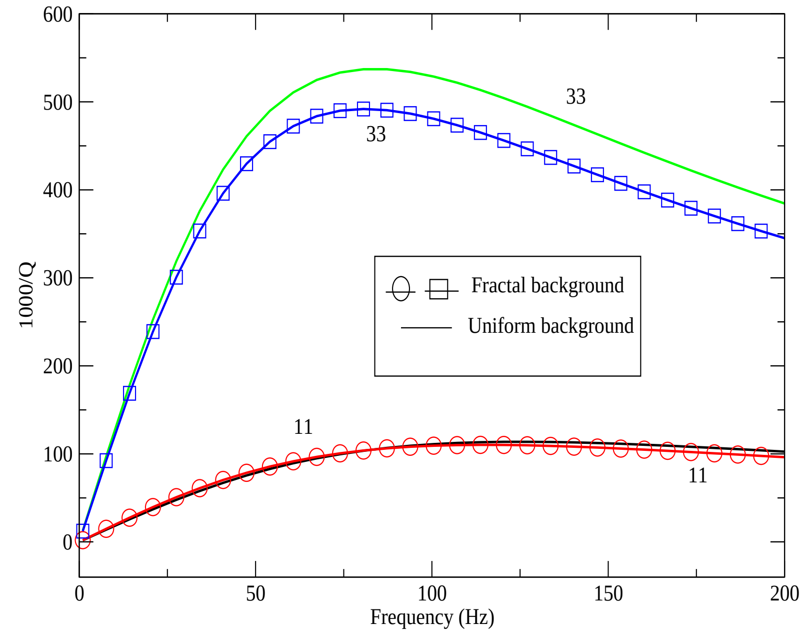

“11” and “33” refer to the qP wave along and perpendicular to the fracture plane. Phase velocities are lower for the fractal case for both “11” and “33” qP waves. Concerning attenuation, for qP “33” waves is lower than in the uniform background case, while attenuation for qP “11” waves is not affected by the fractal background.

CONCLUSIONS.

- Schoenberg's theory predicts that an homogeneous background containing a dense set of horizontal parallel fractures behaves like a TIV medium at long wavelengths.
- We presented a collection of novel FE harmonic experiments to test and validate the theory.
- The methodology was applied to a case where there is no analytical solution, such as fractal variations of the fracture compliances at different pore pressures and fractal Lamé parameters.
- In particular, it is shown that attenuation can be an indicator of overpressure with higher values at high pore pressures.

AKNOWLEDGEMENTS.

I give special thanks to professor Yalchin Efendiev for inviting me to present this work in the 2012 KAUST-IAMCS WORKSHOP.

I also mention the great support of all the people at ISC-TAMU and KAUST in dealing with all the paperwork needed to get me here.

THANKS FOR YOUR ATTENTION !!!!